

Quantitative evaluation of breast density using a dual-energy technique on a digital breast tomosynthesis system

Kun-Mu Lu¹ | Da-Ming Yeh^{2,3} | Bi-Hui Cao⁴ | Chia-Yi Lin² | Chih-Yu Liang^{5,6,7} | Yu-Bo Zhou⁸ | Chia-Jung Tsai⁶

¹Department of Radiology, Shin Kong Wu Ho-Su Memorial Hospital, Taipei City, Taiwan

²Department of Medical Imaging, Chung Shan Medical University Hospital, Taichung City, Taiwan

³Department of Medical Imaging and Radiological Sciences, Chung Shan Medical University, Taichung City, Taiwan

⁴Department of Radiology, The Second Affiliated Hospital of Guangzhou Medical University, Guangzhou, China

⁵Department of Information Engineering, I-Shou University, Kaohsiung City, Taiwan

⁶Department of Medical Imaging and Radiological Sciences, I-Shou University, Kaohsiung City, Taiwan

⁷Department of Emergency Medicine, EDA Hospital, I-Shou University, Kaohsiung City, Taiwan

⁸Department of Library, Guangzhou Medical University, Guangzhou, China

Author to whom correspondence should be addressed. Chia-Jung Tsai
E-mail: cjtsai@isu.edu.tw; Telephone: +886-7-6151100 ext. 7819; Fax: +886-7-6155150.

Funding information

Chung Shan Medical University Hospital, Grant/Award Number: CSH-2009-A-004; Shin Kong Wu Ho-Su Memorial Hospital, Grant/Award Number: SKH-8302-103-0602

Abstract

Purpose: Although breast density is considered a strong risk factor of breast cancer, its quantitative assessment is difficult. To investigate a quantitative method of measuring breast density using dual-energy mammographic imaging with central digital breast tomosynthesis in physically uniform and nonuniform phantoms.

Material and methods: The dual-energy imaging unit used a tungsten anode and silver filter with 30 kVp for high-energy images and 20 kVp for low-energy images. Uniform glandular-equivalent phantoms were used to calibrate a dual-energy based decomposition algorithm. The first study used uniform breast phantoms which ranged in thicknesses from 20 to 70 mm, in 10-mm increments, and which provided 30%, 50%, and 70% of breast density. The second study used uniform phantoms ranging from 10% to 90% of breast density. The third study used non-uniform phantoms (at an average density of 50%) with a thickness which ranged from 20 to 90 mm, in 10-mm increments.

Results: The root mean square error of breast density measurements was 2.64–3.34% for the uniform, variable thickness phantoms, 4.17% for the uniform, variable density phantoms, and 4.49% for the nonuniform, variable thickness phantoms.

Conclusion: The dual-energy technique could be used to measure breast density with a margin of error of < 10% using digital breast tomosynthesis.

PACS

87.00.00

KEY WORDS

breast cancer, breast density, digital breast tomosynthesis, dual-energy

1 | INTRODUCTION

Breast cancer is the most common cancer worldwide and is the most frequent cancer among women, with an estimated 1.67 million new cancer diagnoses in 2012 (25% of all cancers). It ranks as the fifth leading cause of death from cancer overall (5,22,000

deaths), as well as the most frequent cause of cancer death in women in less developed regions (3,24,000 deaths; 14.3% of total deaths). It is now the second leading cause of cancer death in more developed regions (1,98,000 deaths; 15.4% of total deaths), after lung cancer.¹ Boyd et al hold the view that breast density, the percentage of glandular breast tissue, is a strong risk factor

This is an open access article under the terms of the Creative Commons Attribution License, which permits use, distribution and reproduction in any medium, provided the original work is properly cited.

© 2019 The Authors. *Journal of Applied Clinical Medical Physics* published by Wiley Periodicals, Inc. on behalf of American Association of Physicists in Medicine.

for breast cancer. A recent study has found that the risk of breast cancer is four to five times higher in women whose glandular density is higher than 75% than in those with breast density less than 25%.² The possibility of predicting future disease occurrence in individuals could be applicable not only to the design and application of preventive plans but also to interventional trials and clinical decision making.³ Therefore, it is important to measure clinical breast density accurately and safely.

John Wolfe, a pioneer in the field of mammography, put forward a well-cited theory of breast patterns as an index of risk for breast cancer in 1976, that of "breast patterns as an index of risk for developing breast cancer".⁴ The current methods used to evaluate breast density include the four-category Breast Imaging Reporting and Data System (BI-RADS) classification system. BI-RADS has demonstrated positive intrareader ($k = 0.79\text{--}0.86$) and interreader ($k = 0.65\text{--}0.91$) agreements, indicating interreader correlation (r) ranging from 0.7 to 0.93, with correlations better for D1 and D4 than for D2 and D3 breast density categories.^{5,6} The reproducibility of BI-RADS is generally poor owing to reader subjectivity in breast density assessment,^{7,8} leading different implications regarding breast cancer risk prediction and choices in screening. To reduce variability and provide an objective measurement of breast density, quantitative approaches were developed for breast density evaluation.

Shepherd et al⁹ developed dual-energy x-ray absorptiometry (DXA) techniques to calculate density on both mammography units and bone densitometers.^{10,11} Ducote et al subsequently investigated the feasibility of dual-energy mammography to measure breast density in simulation and phantom studies.^{12,13} Laidevant et al¹⁴ successfully regressed the protein composition and the thickness of lipid and water material in a phantom trial. These results can be applied directly to actual breast tissue to distinguish muscle, fat, and glandular components. However, the protocol for obtaining these values might not be applicable to clinical practice as it could possibly produce higher than recommended radiation doses that are not in compliance with international "as low as reasonably achievable" (ALARA) principles. The researchers mentioned above used uniform phantoms for their experiments; few researchers have focused on nonuniform materials and further studies are still necessary for heterogeneous bodies.

Digital breast tomosynthesis (DBT) is rapidly gaining in popularity worldwide due to its high spatial-resolution tomographic images of the breast and its ability to create reconstructions using multiple low-dose projection images.¹⁵ Early clinical trials show improved sensitivity and specificity of DBT compared with digital mammography (DM).^{16,17} Bakic et al¹⁸ determined that breast density may be accurately estimated using central DBT and found substantial inter- and intrareader agreement in breast density estimation between DM and central DBT projection images. Our aim is to investigate the feasibility of the dual-energy technique for quantifying breast density in uniform and nonuniform phantoms using a central DBT system.

2 | MATERIALS AND METHODS

2.A | Dual energy decomposition and calibration

It is possible to combine low- and high-energy images to enhance a particular component in a projection image. However, the presence of nonlinear effects precludes the use of linear log subtraction for generating accurate quantitative dual-energy images. According to Kappadath et al,¹⁹ a linear function failed to model both the thickness and glandular ratio. On the contrary, quadratic, cubic, and conic functions could be adequately modeled. For this reason, a cubic model with 13 coefficients should be used for dual-energy calibration. The cubic equation we used [eq. (1)] was:

$$t = a_1 + a_2 A_{HE} + a_3 R + a_4 T + a_5 A_{HE}^2 + a_6 R^2 + a_7 T^2 + a_8 A_{HE} R + a_9 A_{HE} T + a_{10} R T + a_{11} A_{HE}^3 + a_{12} R^3 + a_{13} T^3 \quad (1)$$

where t (mm) represents the measured glandular thickness, A_{HE} the log-signal functions for high-energy, R the ratio of the log-signal function for low-energy and high-energy ($R = A_{LE}/A_{HE}$), and T (mm) the total thickness, using a nonlinear least-squares minimization algorithm (Levenberg-Marquardt).²⁰

Calibrations were carried out at clinically relevant breast thicknesses using pure adipose and pure glandular phantoms (Computerized Imaging Referencing Systems, Inc. [CIRS], Norfolk, VA, USA). Eighteen points were selected for dual-energy calibration, which included uniform phantoms with thicknesses of 2–9 cm. The uniform phantoms represented either pure glandular tissue (100% density) or pure adipose tissue (0% density). These measurements were used to build a model and determine the coefficient index (Table 1) for eq. (1).

2.B | Phantom studies

Three phantom configurations of uniform- and nonuniform phantoms (model 014A and model 020, CIRS, Norfolk, VA, USA) were

TABLE 1 Fitting coefficients of glandular tissue for dual-energy calibration

Coefficient index	
a_1	547.5679
a_2	−3.9033
a_3	−2227.0
a_4	44.9791
a_5	−3.0621
a_6	2091.5
a_7	−1.7670
a_8	83.8225
a_9	−5.0640
a_{10}	−1.1086
a_{11}	0.0671
a_{12}	−792.6471
a_{13}	0.0433

investigated. The first study used three groups of uniform phantoms (30%, 50%, and 70% density) with known thicknesses of 20–70 mm, in 10-mm increments. The second study used uniform phantoms ranging from 10% to 90% density, at 5% intervals, with thickness varying from 15 to 100 mm (we used a 54% phantom rather than a 55% phantom due to material availability) (Table 2). The third study used nonuniform phantoms with an average density of 50%, ranging in thickness from 20 to 90 mm, in 10-mm increments.

2.C | Image acquisition and processing

A commercial DBT unit (Selenia™ Dimensions™ System; Hologic, Bedford, MA, USA) was used for image acquisition. The device was equipped with a tungsten (W) anode x-ray tube and x-ray filters of rhodium (Rh), silver (Ag), and aluminum (Al). Different filters produce optimal x-ray spectra on the basis of breast thickness, breast composition, and the desired imaging mode. In this study, an Ag filter was selected to increase spectral separation for the high-energy beam in a dual-energy composition.¹² Central DBT imaging was acquired at 0-degree projection with a spatial resolution of 70 μm per pixel using a detector with a $24 \times 29\text{-cm}^2$ field of view, corresponding to a 3328×4096 matrix. As in Feng and Sechopoulos,²¹ high-energy images were set at 30 kVp and 100 mAs, a clinical protocol for an “average” breast. The low-energy images were acquired at 20 kVp and 25 mAs, the lowest available setting on the DBT system.²² For central DBT, the breast phantoms were positioned for the craniocaudal view and were compressed using a standard force of 11 daN. We repeated this study three times during three months, acquiring a total of 129 measurements.

TABLE 2 Thicknesses and densities used in the second phantom study

Known density	Total thickness (mm)
10%	15
15%	20
20%	30
25%	20
30%	60
35%	20
40%	40
45%	60
50%	80
54%	25
60%	40
65%	100
70%	70
75%	60
80%	30
85%	20
90%	15

Mean glandular dose (MGD), the average value of absorbed dose in the breast with glandular tissue, was also used for an estimation of radiation-induced breast cancer risk from mammography. It can be calculated from the eq. (2):

$$\text{MGD} = \text{ESE} \times D_{gN} \quad (2)$$

where ESE, i.e., entrance skin exposure, is expressed in roentgens (R), and D_{gN} is the normalized dose conversion factor in mGy/R resulting from an incident exposure in air of 1R, being a function of breast density, breast thickness, X-ray beam quality (i.e., tube potential and half-value layer), and anode/filter combination.

All image processing was performed using MATLAB software, version 7.10.0.499 (MathWorks, Natick, MA, USA). All uniform and nonuniform materials were measured for both thickness and density, providing an accurate estimation.

2.D | Density measurement

As images were acquired and dual-energy decomposition was performed, each pair of low- and high-energy images was used to translate glandular and adipose material from pixels into thickness. A region of interest (ROI) was established for each image, and the mean glandular thickness (T_g) was measured. The mean measured density (D_m) was calculated by dividing the mean glandular thickness by the total thickness. This value was multiplied by 100 to convert the fractional density to a percentage [eq. (3)]:

$$D_m (\%) = 100 \times \frac{T_g}{T} \quad (3)$$

For the uniform-thickness phantoms, the mean of each phantom image was sampled with a circular ROI (radius of 200 pixels) at the center-of-mass; the standard deviation (SD) was also measured. For the nonuniform phantom study, a user-determined threshold (aimed at attempting to involve the entire phantom) was used when considering the heterogeneous features (Fig. 1). The process of selecting the ROIs was carried out on the high-energy images, and this set of ROIs was used on both low- and high-energy images without modification.

2.E | Error analysis

The root mean square error (RMSE) for density estimation was calculated using eq. (4):

$$\text{RMSE} = \sqrt{\frac{\sum_{i=1}^n (D_{m,i} - D_{k,i})^2}{n}} \quad (4)$$

where D_k represented the known density.

3 | RESULTS

Results for the three phantom studies are tabulated in Tables 3–5. The measured glandular thickness and density are shown as the

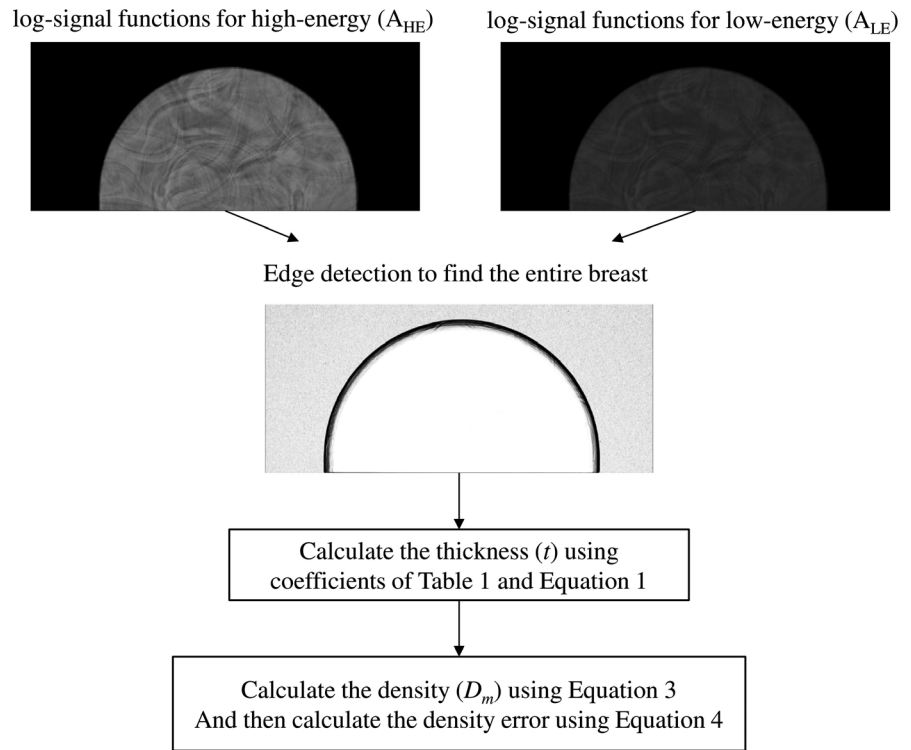


FIG. 1. The flowchart of density measurements in this study

mean value ± SD; the calculating errors are represented by the RMSE. The thickness errors are displayed as the mean value (mm). For the first study (Table 3), the RMSE was 3.34% for 30%

TABLE 3 Errors in density estimation, first study (uniform phantoms of 30%, 50%, and 70% density; root mean square error, 3.34%, 2.64%, and 2.89%, respectively)

Known density	Known thickness (mm)	Measured glandular thickness (mm)	Thickness error (mm)	Measured density (%)
30%	20	7.59 ± 0.56	1.59	34.54 ± 2.55
	30	11.23 ± 0.58	2.23	36.24 ± 1.87
	40	13.32 ± 0.82	1.32	32.48 ± 2.01
	50	15.05 ± 1.03	0.05	29.51 ± 2.03
	60	17.86 ± 1.32	0.14	29.28 ± 2.17
	70	21.90 ± 1.70	0.90	30.85 ± 2.40
	50%	20	11.15 ± 0.41	1.15
30		16.92 ± 0.64	1.92	52.88 ± 2.01
40		22.08 ± 0.75	2.08	53.85 ± 1.83
50		26.98 ± 0.94	1.98	51.88 ± 1.82
60		32.73 ± 1.12	2.73	53.65 ± 1.84
70		36.34 ± 1.47	1.34	51.18 ± 2.07
70%		20	15.77 ± 0.27	1.77
	30	21.17 ± 0.61	0.17	66.17 ± 1.92
	40	29.59 ± 0.70	1.59	72.18 ± 1.72
	50	36.54 ± 0.71	1.54	71.64 ± 1.41
	60	43.58 ± 0.91	1.58	71.44 ± 1.50
	70	50.26 ± 1.17	1.26	69.80 ± 1.49

density, 2.64% for 50% density, and 2.89% for 70% density, while the corresponding mean measured density was 32.15%, 52.36%, and 71.06%, respectively. For the second study (Table 4), the RMSE was 4.17% for all known-density phantoms. The glandular thickness and density errors were approximately 0.52 mm and 0.18%, respectively. For the third study, the results from the nonuniform phantoms (Table 5) had a mildly higher error value, with an RMSE of 4.49%; the averaged errors of measured glandular thickness were 2.70 mm. The averaged density error for all three studies was 3.66%. The results of the density measurements for all three studies are shown in the Fig. 2. The slope and goodness-of-fit (R^2) values of linear regression were 0.95 (95% confidence interval, 0.913–1.006) and 0.97, respectively. The relation between known (K) and estimated (E) densities was calculated using the equation: $E = 0.95 K + 3.54$.

4 | DISCUSSION

Breast density is one of the strongest predictors of breast cancer risk. The extent of breast density can be modified by several factors. Increasing age and menopause²³ are independent contributors to a decrease in breast density.²⁴ Elevated body mass index has been associated with low breast density, whereas increased age at first childbirth has been associated with high breast density.²⁵ Pregnancy at an early age decreases breast density, and this beneficial effect appears to be permanent.²⁶ Postmenopausal hormonal therapies that include both estrogen and progesterone are associated with an increase in breast density that decreases upon discontinuation of therapy.²⁷ Intervention trials have shown that decreases in breast

TABLE 4 Errors in density estimation, second study (uniform phantoms; root mean square error, 4.17%)

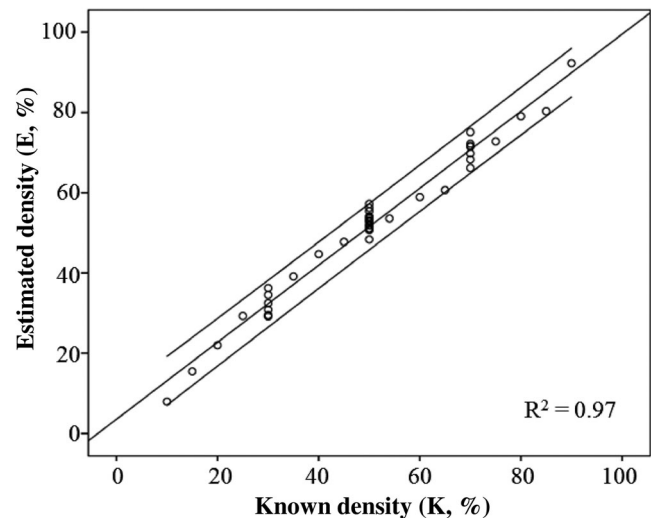
Known density	Known glandular thickness (mm)	Measured glandular thickness (mm)	Thickness error (mm)	Measured density (%)	Density error (%)
10%	1.5	1.35 ± 0.11	0.15	7.93 ± 0.64	2.07
15%	3	3.40 ± 0.31	0.40	15.45 ± 1.40	0.45
20%	6	6.81 ± 0.60	0.81	21.99 ± 1.95	1.99
25%	5	6.44 ± 0.53	1.44	29.27 ± 2.40	4.27
30%	18	17.79 ± 1.32	0.21	29.17 ± 2.16	0.83
35%	7	8.61 ± 0.47	1.61	39.13 ± 2.13	4.13
40%	16	18.32 ± 0.81	2.32	44.69 ± 1.98	4.69
45%	27	29.12 ± 1.18	2.12	47.74 ± 1.94	2.74
50%	40	41.24 ± 1.76	1.24	50.92 ± 2.17	0.92
54%	13.5	14.46 ± 0.44	0.96	53.57 ± 1.65	0.43
60%	24	24.14 ± 0.71	0.14	58.90 ± 1.74	1.10
65%	65	61.27 ± 0.93	3.73	60.66 ± 0.92	4.34
70%	49	49.16 ± 1.17	0.16	68.28 ± 1.30	1.72
75%	45	45.12 ± 0.90	0.12	72.78 ± 1.45	2.22
80%	24	24.51 ± 0.56	0.51	79.08 ± 1.81	0.92
85%	17	16.86 ± 0.20	0.14	80.32 ± 0.97	4.68
90%	13.5	14.76 ± 0.48	1.26	92.28 ± 3.03	2.28

TABLE 5 Errors in density estimation, third study (nonuniform phantoms of 50% density; root mean square error, 4.49%)

Known thickness (mm)	Measured glandular thickness (mm)	Thickness error (mm)	Measured density (%)
20	12.37 ± 1.80	2.37	56.24 ± 8.18
30	16.60 ± 2.86	1.60	51.90 ± 8.96
40	23.45 ± 3.34	3.45	57.20 ± 8.15
50	27.52 ± 4.24	2.52	52.93 ± 8.16
60	32.94 ± 4.81	2.94	53.14 ± 7.76
70	39.89 ± 5.49	4.89	55.41 ± 7.62
80	44.38 ± 5.96	4.38	54.12 ± 7.25
90	44.47 ± 5.74	0.53	48.34 ± 6.24

density are associated with tamoxifen treatment.²⁸ a therapy proven to decrease breast cancer risk. Therefore, some qualitative and quantitative methods involve grading of mammographic density.

Digital breast tomosynthesis is gaining approval as a tool for the evaluation of breast density as well as an adjunct to digital mammography in screening. Ekpo et al²⁹ point out that the investigation and measurement of breast density has been evolving for more than 30 years. FFDM has been frequently used for earlier breast density surveys in simulation¹² or phantom¹³ studies. However, comparing DBT to FFDM reveals several merits to the former, even though the latter is more commonly used. First, DBT shows a stronger correlation of breast density to the parenchymal texture features than DM.³⁰ These results may be reasonable, as DBT takes the whole breast into consideration and acquires

**FIG. 2.** Density measurements for all three phantom studies. The known (K) and estimated (E) densities are related using $E = 0.95 K + 3.54$ with 95% confidence interval of 0.913–1.006. The goodness-of-fit (R^2) value of linear regression was 0.97.

details of depth from the tomographic breast. Additionally, the recall rates for noncancer cases significantly decrease with the addition of tomosynthesis to DM.^{31–33} Our selection of DBT may be well founded, as our results are persuasive when combined with previous research. Ducote et al¹³ accurately used uniform phantoms to quantify breast density with a dual-energy based decomposition algorithm. The present study also showed good functionality for the use of the dual-energy technique for breast density evaluation in uniform and nonuniform phantoms using a

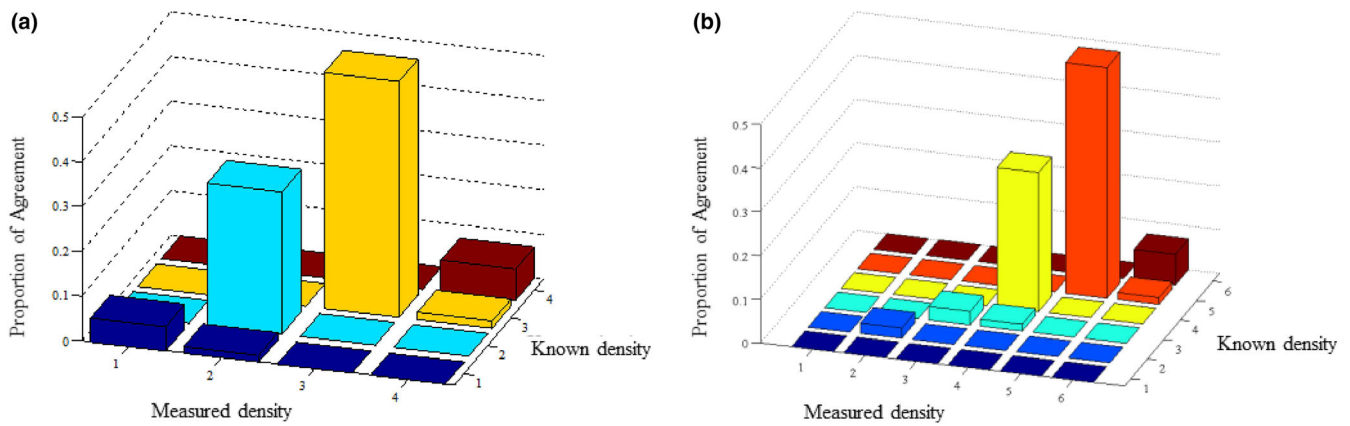


FIG. 3. Graph shows consistent agreement between the categoric estimates of breast density using the Breast Imaging Reporting and Data System (BI-RADS) classification (a) and the Boyd six-grade classification (b)

central DBT system. Previous study by Ducote found a RMSE for breast density measurements of 0.44% (our range, 2.64%–3.34% for three glandular densities) for variable thickness phantoms and 0.64% (our value, 4.17%) for variable density phantoms. Although our results differed slightly, this might be explained by the two following reasons: (a) our study aimed to use a clinically feasible protocol; hence, our use of both high-energy and low-energy images (30 and 20 kVp [the lowest available on the Hologic DBT]) apparently reduced the separation in mean energy between the two beams. Ducote et al used 49 and 28 kVp for their images,¹³ resulting in lower errors. (b) A correction for x-ray scatter was absent in our study, even though this is the predominant source of error in breast density measurement.^{34,35} Encouragingly, even the nonuniform phantoms (well-matched to actual breast tissue in density composition), in which we expected more systematic error, yielded a relatively ideal result with a RMSE value of only 4.49% (compared with 4.17% in uniform phantoms), even though this was the first used of a commercial DBT unit for breast density evaluation (Table 5).

At present, the classical Wolfe four-grade (BI-RADS) system and the Boyd six-grade classification are indispensable in clinical breast density grading. The distribution of calculated breast density on central DBT with dual energy projections in the Wolfe and Boyd systems is shown in the Fig. 3. BI-RADS and Boyd six-grade classifications would result in four overestimations using our data. From the standpoint of BI-RADS [Fig. 3(a)] and Boyd six-grade [Fig. 3(b)] classification, the known glandular densities of 20% and 70% belong to class 1 vs class 3, and class 3 vs class 5, respectively, whereas the corresponding measured 25% and 76% densities in these categories can be assigned to class 2 vs class 4, and class 4 vs class 6. The overestimation in the lower and upper quadrants might result from the absence of scatter correction and the inherent higher recall rate for patients with dense breast tissue because of radiologic tumor masking.² A previous study¹⁸ investigates this variance by measuring the percent density (PD) in 39 women using FFDM and DBT. Three readers estimated

quantitative PD values and six-class Boyd categories, and repeated the study after 8 months, showing a high correlation and substantial agreement between PD on DM and on central DBT projections. However, this study analyzed breast density with only the semiquantitative technique, and uncertainty in the correlation between DM and DBT should be considered due to subjective bias. In our study, the automatic quantitative method was employed, thus eliminating the subjective effect.

For 50% glandular density and a thickness of 5 cm, the total summarized MGD in dual-energy images is 1.78 mGy for uniform and 1.81 mGy for nonuniform phantoms. By comparison, the average MGD for screening mammography in the United States in 2006 was 1.8 mGy for a reference phantom equivalent to 50% density and 4.7 cm thickness.³⁶ In a study of five DM systems, the MGD varied from 1.4 to 2.4 mGy for 1-view screening mammography.³⁷ The dual-energy DBT used in our study results in a dose comparable to that of routine DM. There are some limitations in this study; the first, regression coefficients in Table 1 such as A_{HE} or R value might be changed depending on detector type (Y6- or Y8), software version and calibration. So, other coefficients could be taken into consideration for modification breast density accuracy in the future. Another limitation is the absence of an x-ray scatter correction, which is the predominant source of error in breast density measurement using dual energy mammography. In addition, we used a newly proposed algorithm for which more study is needed to verify efficacy. Future clinical implementation of this technique is expected using a clinical protocol in which automatic exposure control, as high-energy imaging, is combined with low-dose 3D projection, as low-energy imaging. Previously, some 2D interactive computer programs have also been used to generate a percentage mammographic density.^{5,38,39} These methods, as well as other similar interactive computer and qualitative estimates, assess a 3D organ using 2D techniques, so are likely to be limited. Therefore, DBT potentially has sufficient superiority, which provides 2D and 3D imaging for diagnosis while offering quantification of breast density as a risk factor for breast cancer.

5 | CONCLUSIONS

In conclusion, the RMSE for breast density measurements was 2.64–3.34% for uniform, variable thickness phantoms, 4.17% for uniform, variable density phantoms, and 4.49% for nonuniform, variable thickness phantoms. The results of these phantom studies indicate that the dual-energy technique can be used to measure breast density with an error of < 10%, using DBT.

ACKNOWLEDGMENTS

This study was financially supported in part by a grant from Chung Shan Medical University Hospital (grant number: CSH-2009-A-004) and by a grant from Shin Kong Wu Ho-Su Memorial Hospital (grant number: SKH-8302-103-0602).

CONFLICT OF INTEREST

The authors declare no competing financial interests.

REFERENCES

- Ferlay J, Soerjomataram I, Dikshit R, et al. Cancer incidence and mortality worldwide: sources, methods and major patterns in GLOBOCAN 2012. *Int J Cancer*. 2015;136:E359–E386.
- Boyd NF, Guo H, Martin LJ, et al. Mammographic density and the risk and detection of breast cancer. *N Engl J Med*. 2007;356:227–236.
- Freedman AN, Seminara D, Gail MH, et al. Cancer risk prediction models: A workshop on development, evaluation, and application. *J Natl Cancer Inst*. 2005;97:715–723.
- Wolfe JN. Breast patterns as an index of risk for developing breast cancer. *AJR Am J Roentgenol*. 1976;126:1130–1137.
- Tagliafico A, Tagliafico G, Astengo D, et al. Mammographic density estimation: one-to-one comparison of digital mammography and digital breast tomosynthesis using fully automated software. *Eur Radiol*. 2012;22:1265–1270.
- Tagliafico AS, Tagliafico G, Cavagnetto F, Calabrese M, Houssami N. Estimation of percentage breast tissue density: comparison between digital mammography (2D full field digital mammography) and digital breast tomosynthesis according to different BIRADS categories. *Br J Radiol*. 2013;86:20130255.
- Gweon HM, Youk JH, Kim JA, Son EJ. Radiologist assessment of breast density by BI-RADS categories versus fully automated volumetric assessment. *AJR Am J Roentgenol*. 2013;201:692–697.
- Redondo A, Comas M, Macià F, et al. Inter- and intraradiologist variability in the BI-RADS assessment and breast density categories for screening mammograms. *Br J Radiol*. 2012;85:1465–1470.
- Shepherd JA, Herve L, Landau J, Fan B, Kerlikowske K, Cummings SR. Novel use of single x-ray absorptiometry for measuring breast density. *Technol Cancer Res Treat*. 2005;4:173–182.
- Shepherd JA, Herve L, Landau J, Fan B, Kerlikowske K, Cummings SR. Clinical comparison of a novel breast DXA technique to mammographic density. *Med Phys*. 2006;33:1490–1498.
- Shepherd JA, Kerlikowske KM, Smith-Bindman R, Genant HK, Cummings SR. Measurement of breast density with dual X-ray absorptiometry: feasibility. *Radiology*. 2002;223:554–557.
- Ducote JL, Molloy S. Quantification of breast density with dual energy mammography: A simulation study. *Med Phys*. 2008;35:5411–5418.
- Ducote JL, Molloy S. Quantification of breast density with dual energy mammography: an experimental feasibility study. *Med Phys*. 2010;37:793–801.
- Laidevant AD, Malkov S, Flowers CI, Kerlikowske K, Shepherd JA. Compositional breast imaging using a dual-energy mammography protocol. *Med Phys*. 2010;37:164–174.
- Sia J, Moodie K, Bressel M, et al. A prospective study comparing digital breast tomosynthesis with digital mammography in surveillance after breast cancer treatment. *Eur J Cancer*. 2016;61:122–127.
- Hodgson R, Heywang-Köbrunner SH, Harvey SC, et al. Systematic review of 3D mammography for breast cancer screening. *Breast*. 2016;27:52–61.
- Chae EY, Kim HH, Cha JH, Shin HJ, Choi WJ. Detection and characterization of breast lesions in a selective diagnostic population: diagnostic accuracy study for comparison between one-view digital breast tomosynthesis and two-view full-field digital mammography. *Br J Radiol*. 2016;89:20150743.
- Bakic PR, Carton AK, Kontos D, Zhang C, Troxel AB, Maidment AD. Breast percent density: estimation on digital mammograms and central tomosynthesis projections. *Radiology*. 2009;252:40–49.
- Kappadath SC, Shaw CC. Dual-energy digital mammography: calibration and inverse-mapping techniques to estimate calcification thickness and glandular-tissue ratio. *Med Phys*. 2003;30:1110–1117.
- Levenberg KQ. A method for the solution of certain non-linear problems in least squares. *Q Appl Math*. 1944;2:164–168.
- Feng SS, Sechopoulos I. Clinical digital breast tomosynthesis system: dosimetric characterization. *Radiology*. 2012;263:35–42.
- Tsai CJ, Chen RC, Peng HL, Hsu WL, Lee JJ. Improved microcalcification visualization using dual-energy digital mammography. *Acta Radiol*. 2013;54:614–621.
- Kerlikowske K, Grady D, Barclay J, Sickles EA, Ernster V. Effect of age, breast density, and family history on the sensitivity of first screening mammography. *JAMA*. 1996;276:33–38.
- Boyd N, Martin L, Stone J, Little L, Minkin S, Yaffe M. A longitudinal study of the effects of menopause on mammographic features. *Cancer Epidemiol Biomarkers Prev*. 2002;11:1048–1053.
- White E, Velentgas P, Mandelson MT, et al. Variation in mammographic breast density by time in menstrual cycle among women aged 40–49 years. *J Natl Cancer Inst*. 1998;90:906–910.
- Vachon CM, Kuni CC, Anderson K, Anderson VE, Sellers TA. Association of mammographically defined percent breast density with epidemiologic risk factors for breast cancer (United States). *Cancer Causes Control*. 2000;11:653–662.
- Persson I, Thurffjell E, Holmberg L. Effect of estrogen and estrogen-progestin replacement regimens on mammographic breast parenchymal density. *J Clin Oncol*. 1997;15:3201–3207.
- Atkinson C, Warren R, Bingham SA, Day NE. Mammographic patterns as a predictive biomarker of breast cancer risk: effect of tamoxifen. *Cancer Epidemiol Biomarkers Prev*. 1999;8:863–866.
- Ekpo EU, McEntee MF. Measurement of breast density with digital breast tomosynthesis - a systematic review. *Br J Radiol*. 2014;87:20140460.
- Skaane P, Bandos AI, Gullien R, et al. Comparison of digital mammography alone and digital mammography plus tomosynthesis in a population-based screening program. *Radiology*. 2013;267:47–56.
- Sumkin JH, Ganott MA, Chough DM, et al. Recall rate reduction with tomosynthesis during baseline screening examinations: an assessment from a prospective trial. *Acad Radiol*. 2015;22:1477–1482.
- Destounis S, Arieno A, Morgan R. Initial experience with combination digital breast tomosynthesis plus full field digital mammography

- or full field digital mammography alone in the screening environment. *J Clin Imaging Sci.* 2014;4:9.
33. Carbonaro LA, Di Leo G, Clauser P, et al. Impact on the recall rate of digital breast tomosynthesis as an adjunct to digital mammography in the screening setting. A double reading experience and review of the literature. *Eur J Radiol.* 2016;85:808–804.
 34. Leon SM, Brateman LF, Wagner LK. Characterization of scatter in digital mammography from physical measurements. *Med Phys.* 2014;41:061901.
 35. Lu Y, Peng B, Lau BA, et al. A scatter correction method for contrast-enhanced dual-energy digital breast tomosynthesis. *Phys Med Biol.* 2015;60:6323–6354.
 36. Spelic D, Kaczmarek R, Hilohi M, Belella S. United States radiological health activities: inspection results of mammography facilities. *Biomed Imaging Interv J.* 2007;3:e35.
 37. Williams MB, Raghunathan P, More MJ, et al. Optimization of exposure parameters in full field digital mammography. *Med Phys.* 2008;35:2414–2423.
 38. Tagliafico A, Tagliafico G, Tosto S, et al. Mammographic density estimation: comparison among BI-RADS categories, a semi-automated software and a fully automated one. *Breast.* 2009;18:35–40.
 39. Tagliafico A, Calabrese M, Tagliafico G, et al. Increased mammographic breast density in acromegaly: quantitative and qualitative assessment. *Eur J Endocrinol.* 2011;164:335–340.